Homogenization of Corrugate Core Sandwich Structures for ITPS Applications

Nazim Khan[1]
Pritam Chakraborty[2]

Abstract

The corrugated core sandwich structure is being considered for the Integrated Thermal Protection System (ITPS) of Reusable Launch Vehicles (RLVs) since it is thermally insulative and has a better specific load-carrying capability than conventional TPS. However, the analyses of the RLVs components such as wings, fuselage, etc., along with the ITPS panel may become computationally infeasible. This can be resolved by considering the corrugated structure as a homogenized orthotropic plate for performing the structural simulations of such components. However, a thicknesswise temperature gradient can exist in the ITPS during flight conditions (such as ascent and re-entry phase) and can have significantly different temperature distribution depending on their position on the vehicle, which if not incorporated during homogenization may render the orthotropic plate properties inaccurate and the results from analysis erroneous. In this work, the homogenization method with a thicknesswise temperature gradient is developed to predict the temperature-dependent homogenized properties of the ITPS panel. The novelty of this work is the incorporation of spatially varying temperature gradient in the homogenous model. The comparisons show that the homogenized plate representation derived in this work is useful for an accurate and efficient structural analysis.

Keywords: *ITPS panel, corrugated core sandwich structures, temperature gradient, homogenization.*

[1] *Department of Aerospace Engineering, Indian Institute of Technology, Kanpur, Uttar-Pradesh, 208016.*

Introduction

The low-cost space access can be achieved by the development of the fully Reusable Launch Vehicles (RLVs) by increasing the operational extensibility for multiple regular missions (Bekey et al., 1994). RLVs are subjected to varying loads during flight operation from ascent to re-entry phase. Thermal Protection Systems (TPSs) are being used on the exterior surface of RLVs to prevent heat into the vehicle interior during the aerodynamic re-entry. However, one of the major drawbacks of TPSs is their low load-carrying capacity (Martinez et al., 2007; Sharma et al., 2010). Furthermore, TPSs accounts for the major part of launch weight must be lightweight to keep the minimal launch cost. To address these drawbacks, multifunctional ITPSs are currently being developed, which combines the TPSs functions and load carrying capabilities into a single structure. Additionally, ITPSs should be reusable, operable, have high stiffness to weight ratio, good energy absorbing and thermal insulation capabilities (Satish et al., 2006; Sharma et al., 2010).

The core geometry of the ITPS panel can be chosen from foam, honeycomb, truss, or corrugated core geometries. The honeycomb core has high specific stiffness as compared to the foam core (Yang et al., 2019). However, debonding may occur at the interface of the core and face sheets due to a small adhesive area. This issue can be sorted out by the corrugated core sandwich structure, which can resist bending and twisting in addition to vertical shear (Chang et al., 2005). The truss core sandwich structure is even lighter and more competent to carry the compressive and bending load as compared to the corrugated core. However, forces generated by large thermal gradient cannot withstand by truss core geometry. Thus, it makes them unsuitable for ITPS applications (Bapanapalli et al., 2007). The previous studies (Bapanapalli et al., 2007; Martinez et al., 2007; Sharma et al., 2010) have been proved that the corrugated core sandwich structure has better specific load-bearing capabilities than conventional TPS. Hence, the corrugated core sandwich structure is one such ITPS design that is currently being explored.

The ITPS panel is composed of several unit-cells as shown in Figure 1. It consists of two stiff face sheets separated by a lightweight thick core. The corrugated core keeps the face sheets apart and facilitates the sandwich panel as a thick plate by resisting the vertical deformation, shear strain and curvature in the longitudinal direction (Chang et al., 2005). The empty space in the corrugated core is filled with insulating material to obstruct the heat transfer from the top face sheet (TFS) to the bottom face sheet (BFS) (Bapanapalli et al., 2007).

Figure 1: Corrugated Core Sandwich Panel for ITPS

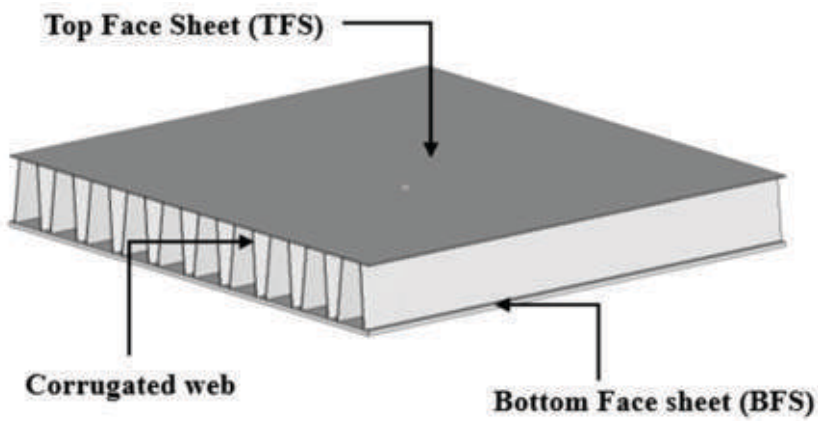

Structural analysis of RLVs with ITPS can be a very challenging task as the length scale of the structural components of the RLV (such as wings, fuselage, etc.) are significantly larger than the length scale of the core. Thus, the incorporation of the core geometry in the analysis may lead to an exorbitant computational cost. This necessitates the derivation of the homogenous representation of corrugated sandwich structure such that Finite Element Analysis (FEA) of structural components is computationally feasible.

The homogenization of the corrugated core sandwich structure as a thick plate was first proposed by Libove and Hubka (1951). They determined the equivalent extensional, bending, and transverse shear stiffnesses using force and distortion relationship and conducted the experimental study to compare the bending, transverse and twisting stiffnesses with good accuracy. A similar technique was adopted for the homogenization of c-core, z- core and truss-core sandwich plate (Fung et al., 1993; Fung et al., 1994; Lok et al., 2000). A comparison of maximum deflection under uniform distributed load was done with numerical analyses and analytical results. Nordstrand et al. (1994) derived the analytical expression for shear moduli and showed the variation with the corrugation shape. The shear modulus along the corrugation is determined by considering both rigid as well as deformable face-sheets and quantified the reduction due to elastic facing. The shear modulus across the corrugation is determined by assuming the deformation of the core only. The comparison was done using FEA and previous analytical solution (Libove and Hubka) with reasonable accuracy and concluded that shear modulus is very sensitive to the corrugation shape. Carlsson et al. (2001) enhanced the previous analytical models using the First Order Shear Deformation Theory (FSDT). The equivalent stiffness properties were evaluated and compared with the experimental results, and concluded that extensional and bending stiffness properties are dominated by face-sheets. While the transverse shear stiffness properties across the corrugation are highly dependent on the corrugation shape. Chang et al. (2005) derived the closed-form solution to represent the bending behavior of the 3D corrugated core sandwich structure as a homogenous thick plate with various boundary conditions based on the Mindlin–Reissner plate theory. The comparison of maximum deflection and moments was done with the experimental results obtained by Tan et al. (1989). Martinez et al. (2007) analytically determined the equivalent stiffness properties using the strain energy approach and homogenized the ITPS panel as an orthotropic plate. The predicted stiffness properties were verified with FE unit-cell analysis by imposing six linearly independent strains. The computed maximum deflection of the three-dimensional (3D) ITPS panel was in good agreement with the homogenized plate model under simply supported boundary conditions subjected to uniform pressure load. Sharma et al. (2010) determined the equivalent stiffness properties of the ITPS panel by imposing the six linearly independent deformations using the periodic boundary conditions and verified these properties of a homogenized plate subjected to uniform pressure load. Li et al. (2019) determined Poisson's ratios and elastic modulus in thickness directions in addition to the in-plane elastic constants of the balanced corrugated core structure. However, the predicted elastic constants were determined by the stretching and shearing of unit-cell without considering the bending effect, which can yield inaccurate results under bending load. They homogenized the corrugated structure as a continuous 3D plate and validated the detailed and equivalent model under displacement control stretching.

The homogenization methods as discussed above were considered the constant temperature throughout the thickness that makes them unusable for RLV analysis. Typically TFS is subjected to severe aerodynamic heating during re-entry. Most of the incident heat of the TFS is radiated out to the ambient and some of the heat is conducted to BFS, resulting in thicknesswise temperature variation. This necessitates the incorporation of temperature-dependent homogenized properties into the homogenous model for accurate analysis. To address

this issue, Collier et al. (1993) and Craig (1994) analytically determined the equivalent properties of the stiffened panel assuming constant temperature gradient across the thickness by considering each constituent of the panel as a lamina based on classical laminated plate theory (CLPT). The equivalent properties were validated using finite element unit-cell analysis with good agreement. However, the shear deformation effect was not considered in their work, which is significant due to the low transverse rigidity of the core. Also, the incompatibility of the deformation of face sheets and core can miscalculate the equivalent properties.

Typically thicknesswise temperature gradient in the ITPS may vary with the spatial position in the vehicle and operating conditions. Thus, it is desirable to incorporate the through-thickness temperature variations and their effect on the properties in the plate theory. In this work, the extension of the plate theory has been proposed by representing the thicknesswise temperature variation in terms of a polynomial. Once, the highest order of temperature polynomial is known, the constants to be calibrated for chosen geometry and material properties can be obtained by unit-cell and Finite Element Method (FEM) based beam analyses. The calibrated plate model can be applied to perform structural analysis for any temperature variation within the maximum polynomial order. Thus, the proposed methodology can be used for the mechanical analysis of the ITPS panel as a homogenous plate model for accurate and efficient analysis.

Micromechanical Analysis

The corrugated core sandwich structure can be idealized as a homogenized thick plate to perform mechanical analysis (Martinez et al., 2007; Sharma et al., 2010). The plate representation replaces the actual model of the ITPS panel by incorporating the temperature-dependent A-B-D and shear stiffness properties. This representation reduces the number of degree of freedom significantly to perform computationally efficient analysis. The in-plane extensional ([A]), coupling ([B]), bending ([D) stiffness matrices and transverse shear stiffness properties (A_{44} and A_{55}) of an orthotropic panel are governed by the following constitutive relations:

$$\begin{Bmatrix} N_x \\ N_y \\ N_{xy} \\ M_x \\ M_y \\ M_{xy} \end{Bmatrix} = \begin{bmatrix} A_{11} & A_{12} & 0 & B_{11} & B_{12} & 0 \\ A_{12} & A_{22} & 0 & B & B_{22} & 0 \\ 0 & 0 & A_{66} & 0 & 0 & B_{66} \\ B_{11} & B_{12} & 0 & D_{11} & D_{12} & 0 \\ B & B_{22} & 0 & D_{12} & D_{22} & 0 \\ 0 & 0 & B_{66} & 0 & 0 & D_{66} \end{bmatrix} \begin{Bmatrix} \varepsilon_{0x} \\ \varepsilon_{0y} \\ \gamma_{0xy} \\ \kappa_x \\ \kappa_y \\ \kappa_{xy} \end{Bmatrix} \quad (1)$$

$$\begin{Bmatrix} Q_x \\ Q_y \end{Bmatrix} = \begin{bmatrix} A_{55} & 0 \\ 0 & A_{44} \end{bmatrix} \begin{Bmatrix} \gamma_{xz} \\ \gamma_{yz} \end{Bmatrix} \quad (2)$$

where, N_x, N_y and N_{xy} are the in-plane forces per unit length, M_x, M_y and M_{xy} are the mid-plane moments per unit length, Q_x and Q_y are the transverse shear forces, ε_{0x}, ε_{0y} and γ_{0xy} are the mid-plane strain components, κ_x, κ_y and κ_{xy} are the mid-plane curvatures, and γ_{xz} and γ_{yz} are the transverse shear strains.

In this work, the methodology described by Sharma et al. (2010) is used to evaluate the homogenized stiffness properties. The smallest repetitive unit of the sandwich structure as shown in Figure 2a is considered for the analysis with chosen geometric and material properties. In this figure, 2p is the length of the unit-cell, $\{\varepsilon_{0x}, \varepsilon_{0y}, \gamma_{0xy}, \kappa_x, \kappa_y, \kappa_{xy}\} = \{1, 0, 0, 0, 0, 0\}$ are enforced to unit-cell FE model shown in Figure 2b to get resultant nodal forces and moments. From these resultant reaction forces and moments as shown in Equation 1, stiffness components were computed as follow: $N_x = A_{11}$, $N_y = A_{12}$ and $M_x = B_{11}$, $M_y = B_{12}$. Other components of stiffness matrices were computed similarly by imposing other macroscopic deformation.

Figure 2: Periodic unit-cell: (a) Geometry, and (b)Edges on which boundary conditions are applied

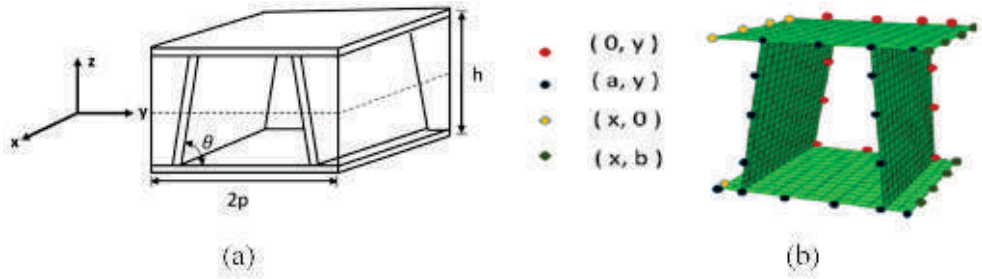

The transverse shear stiffness properties (A_{55} and A_{44}) shown in Equation 2 cannot be obtained from unit-cell analyses because it violates the anti-periodicity of moments. These properties are determined by FEM beam analysis subjected to uniform pressure load as shown in Figure 3a and 3b by comparing the transverse deflection with an analytical solution (Sharma et al., 2010). The expressions of A_{55} and A_{44} as shown in Equations 3 and 4 were obtained by homogenous cantilever beam using the First Order Shear Deformation Theory (FSDT).

Figure 3: FEM model to determine (a) A_{55}, and (b) A_{44}. Faces y = 0 and y = 2p in (a), and faces x = 0 and x = 2p in (b), are under plane strain states.

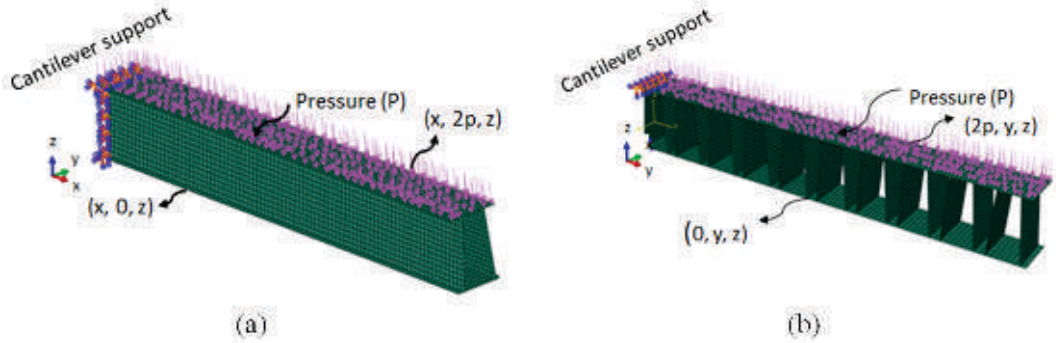

$$A_{55} = \frac{4D_{11}^{*} P\, a^2}{(8wD_{11}^{*} - P\, a^4)} \tag{3}$$

$$A_{44} = \frac{4D_{22}^{*} P\, a^2}{(8wD_{22}^{*} - P\, a^4)} \tag{4}$$

$$\text{Where, } D_{11}^{*} = \left(D_{11} - \frac{{B_{11}}^2}{A_{11}}\right) \text{ and } D_{22}^{*} = \left(D_{22} - \frac{{B_{22}}^2}{A_{22}}\right) \tag{5}$$

Temperature-dependent Homogenized Stiffness Properties

The homogenization method presented in Sharma et al. (2010) donot consider the effect of temperature variation on the homogenized properties. However, the ITPS panel can experience a thicknesswise temperature gradient which can vary with location on the vehicle. This may require repeating the homogenization procedure for the various possible temperature gradients for the chosen geometric and material properties of the constituents. In the proposed method, the homogenized stiffness properties with thicknesswise temperature variation are represented in terms of unknown constants. These constants can be calibrated from few FEM-based unit cell and beam analyses.

In the modified plate model proposed in this work, the temperature-dependent elasticity matrix was assumed to be linearly dependent on temperature as

$$[Q] = [Q_R] + [Q_T]\,(T\text{-}T_R) \tag{6}$$

where, $[Q_R]$ is the in-plane stress elasticity stiffness matrix at a reference temperature, $[Q_T]$ is the slope of in-plane stress stiffness matrix with temperature, T is some temperature and T_R is a reference temperature. The through thickness strain distribution in the plate theory is given by

$$\{\varepsilon\} = \{\varepsilon_0\} + z\{\kappa\} = \begin{Bmatrix}\varepsilon_{0x}\\ \varepsilon_{0y}\\ \gamma_{0xy}\end{Bmatrix} + z\begin{Bmatrix}\kappa_x\\ \kappa_y\\ \kappa_{xy}\end{Bmatrix} \tag{7}$$

The resultant mid-plane forces and moments can be obtained using Equations 1 and 7

$$(\{N\},\{M\}) = \int_{-\frac{h}{2}}^{\frac{h}{2}} \{\sigma\}(1,z)dz = \int_{-\frac{h}{2}}^{\frac{h}{2}} [Q](\{\varepsilon_0\} + z\{\kappa\})(1,z)dz \tag{8}$$

The expansion of Equation 8 yield

$$\begin{Bmatrix}\{N\}\\ \{M\}\end{Bmatrix} = \begin{bmatrix}A & B\\ B & D\end{bmatrix}\begin{Bmatrix}\{\varepsilon_0\}\\ \{\kappa\}\end{Bmatrix} \tag{9}$$

where,

$$[A] = \int_{-\frac{h}{2}}^{\frac{h}{2}} ([Q_R] + [Q_T](T - T_R))z\,dz$$

$$[B] = \int_{-\frac{h}{2}}^{\frac{h}{2}} ([Q_R]z + [Q_T](T - T_R))z^2\,dz \tag{10}$$

$$[D] = \int_{-\frac{h}{2}}^{\frac{h}{2}} ([Q_R]z^2 + [Q_T](T - T_R))z^3\,dz$$

The temperature field can be any order of polynomial depending upon the shape and trajectory of the vehicle such as $T = a_0(x, y) + a_1(x, y)\,z + a_2(x, y)\,z^2 + \ldots\ldots a_n(x, y)\,z^n$, where n is the order of temperature profile. The proposed method has been demonstrated by considering the linear temperature variation along thickness. The homogenized properties [A], [B] and [D] can be obtained by substituting $T = a_0(x, y) + a_1(x, y)\,z$ in Equation 10, as shown below.

$$[A] = [A_R] + \bar{a}_0[A_T] + a_1[B_T]$$

$$[B] = [B_R] + \bar{a}_0[B_T] + a_1[D_T] \tag{11}$$

$$[D] = [D_R] + \bar{a}_0[D_T] + a_1[E_T]$$

where,

$$([A_R],[B_R],[D_R]) = \int_{-\frac{h}{2}}^{\frac{h}{2}} [Q_R](1,z,z^2)dz, \text{ and}$$
$$([A_T],[B_T],[D_T],[E_T]) = \int_{-\frac{h}{2}}^{\frac{h}{2}} [Q_R](1,z,z^2,z^3)\,dz \tag{12}$$

are various constants that have to be calibrated. It is clear from Equation 11 that the temperature-dependent stiffness properties ([A], [B] and [D]) are related to these constants. These constants were determined by performing the unit-cell analyses using three temperature field such that: $\bar{a}_0 = 0$ and $a_1 = 0$; $\bar{a}_0 > 0$ and $a_1 = 0$; $\bar{a}_0 > 0$ and $a_1 > 0$. Using calibrated constants seen in Equation 12, the [A], [B] and [D] can easily be obtained by substituting a_0 and a_1 for any linear temperature field as can be seen from Equation 11.

The expressions of the temperature-dependent transverse shear stiffness properties $(A_{55}$ and $A_{44})$ were derived for linear thicknesswise temperature field $(\mathrm{T} = \mathrm{a}_0 + \mathrm{a}_1 \mathrm{z})$

assuming $Q_{44} = Q_{44}^R + Q_{44}^T(T - T_R)$ and $Q_{55} = Q_{55}^R + Q_{55}^T(T - T_R)$ following

$$A_{55} = \int_{-\frac{h}{2}}^{\frac{h}{2}} Q_{55} dz = \int_{-\frac{h}{2}}^{\frac{h}{2}} \left(Q_{55}^R + Q_{55}^T(T - T_R)\right) dz = A_{55}^R + \bar{a}_0 A_{55}^T + a_1 B_{55}^T$$

$$A_{44} = \int_{-\frac{h}{2}}^{\frac{h}{2}} Q_{44} dz = \int_{-\frac{h}{2}}^{\frac{h}{2}} \left(Q_{44}^R + Q_{44}^T(T - T_R)\right) dz = A_{44}^R + \bar{a}_0 A_{44}^T + a_1 B_{44}^T \quad (13)$$

Where, $(A_{ii}^R, A_{ii}^T, B_{ii}^T) = \int_{-\frac{h}{2}}^{\frac{h}{2}} (Q_{ii}^R, Q_{ii}^T, Q_{ii}^T z) dz$ and i = 4, 5.

FEM based cantilever beam analyses were performed as described earlier using $\bar{a}_0 = 0$ and $a_1 = 0$; $\bar{a}_0 > 0$ and $a_1 = 0$; $\bar{a}_0 > 0$ and $a_1 > 0$ to evaluate calibrated properties (A_{ii}^R, A_{ii}^T and B_{ii}^T). It can be observed from Equation 13 that $A_{ii}^R, A_{ii}^T, B_{ii}^T$ are required for the evaluation of the transverse shear stiffness properties (A_{55} and A_{44}) for any linear thicknesswise temperature field by substituting the value of a_0 and a_1.

The methodology proposed in this work can be extended to any thicknesswise temperature polynomial to predict the homogenized properties. Some additional constants were required to calibrate depending upon the order of the polynomial. In general, the number of FE simulations on unit-cell is to determine [A], [B] and [D], and (4 + 2n) for transverse shear stiffnesses (A_{55} and A_{44}), where $< >$ is Macaulay bracket and n is the order of temperature polynomial.

Calibration and Verification of Homogenized Properties

The homogenization method described in Section 2 was verified for a corrugated core sandwich structure with the geometrical parameters as shown in Table 1.

Table 1: Geometrical Properties of Unit-cell (Sharma, Shankar, & Haftka, 2010)

Parameter	2p, mm	h, mm	$\boldsymbol{\theta}$, deg	$\boldsymbol{t_{TFS}}$, mm	$\boldsymbol{t_{BFS}}$, mm	$\boldsymbol{t_{web}}$, mm
	50	70	85	1.2	7.49	1.63

The material of the TFS and core was chosen to be Ti-6Al-4V ($E = 110$ GPa, $\mu = 0.30$) and the BFS to be Beryllium alloy ($E = 290$ GPa, $\mu = 0.063$). All these geometric and material properties were based on the study performed by Sharma et al. (2010). The temperature-dependent Young's modulus of Ti-6Al-4V and Beryllium alloy given in Sharma et al. (2010), were linearly fitted to obtain T_R, E_R, and E_T for the two materials as shown in Figure 4. In the ITPS sandwich panel, the TFS, BFS and the corrugated core are usually made from different materials. Thus, T_R, E_R, and E_T need not be the same for the different sections. For the homogenization procedure, T_R was considered equal value for each material associated with unit-cell and obtained by interpolation.

Figure 4: Variation of Young's Modulus with Temperature

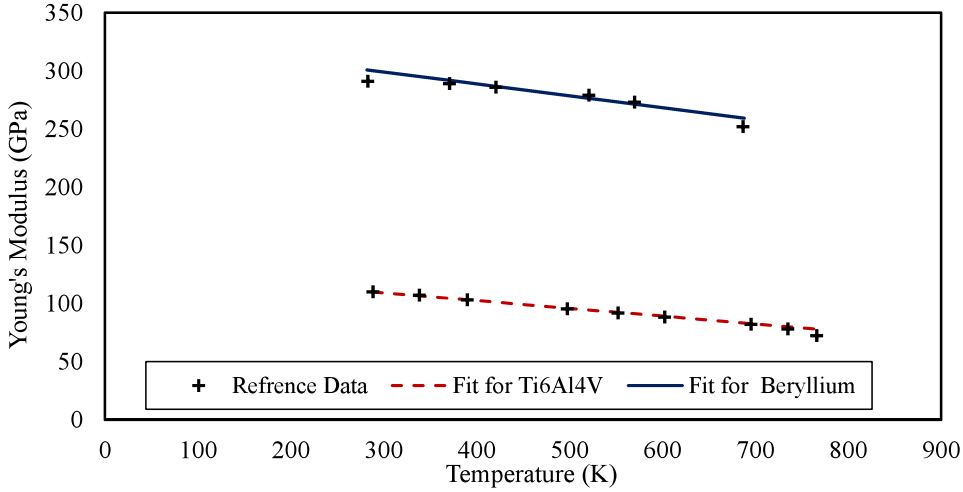

Furthermore, the temperature distribution through the thickness of the ITPS panel need not be a single monotonic function. Rather, it is expected to have different monotonic profiles in the three sections with continuity of temperature and discontinuous gradients at their interfaces. Since the thickness of the corrugated core is very large as compared to the face sheets. Hence, it is assumed, the cross-section of the ITPS has single monotonic temperature distribution across the thickness. The linear fitted constants for Titanium and Beryllium-alloy are shown in Table 2.

Table 2: Linearly Fitted Material Parameters

Material	T_R, K	ER, 10^9 N/mm²	ET, 10^9 N/mm²-K
Ti6Al4V	288	110	-0.067
Beryllium alloy	288	300	-0.138

Calibration of Homogenized Properties

Using these fitted constants as shown in Table 2, the calibrated properties ($[A_R]$, $[B_R]$, $[D_R]$, $[A_T]$, $[B_T]$, $[D_T]$, and $[E_T]$) were evaluated as discussed in Section 2.1. The thicknesswise temperature fields in the unit cell and FE beam analyses were constructed considering $a_0 = 288$ and $a_1 = 0$; $a_0 = 500$ and $a_1 = 0$; $a_0 = 500$ and $a_1 = 5$. Since the TFS and web of this panel are of the same material, the temperature gradients are expected to be continuous between the sections, justifying the evaluation of their constants together. The values of these constants for the core and face sheets (TFS and BFS) together are shown in Tables 3 and 4.

Table 3: Calibrated Properties at the Reference Temperature

$[A_R], 10^6\ N/mm$	$[B_R], 10^6\ N$	$[D_R], 10^6\ N-mm$
$\begin{bmatrix} 2.94 & 0.18 & 0 \\ 0.18 & 2.40 & 0 \\ 0 & 0 & 1.11 \end{bmatrix}$	$\begin{bmatrix} -73.86 & -3.45 & 0 \\ -3.45 & -73.86 & 0 \\ 0 & 0 & 35.25 \end{bmatrix}$	$\begin{bmatrix} 3.15 & 0.22 & 0 \\ 0.22 & 2.94 & 0 \\ 0 & 0 & 1.36 \end{bmatrix}$

Figure 4: Variation of Young's Modulus with Temperature

$[A_T], \frac{10^6 N}{mm-K}$	$[B_T], \frac{10^5 N}{K}$	$[D_T], 10^6 N-mm/K$	$[E_T], 10^6\ Nmm^2/K$
$\begin{bmatrix} -1.17 & -0.76 & 0 \\ -0.76 & -0.084 & 0 \\ 0 & 0 & -0.38 \end{bmatrix}$	$\begin{bmatrix} 23.2 & 0.73 & 0 \\ 0.73 & 23.2 & 0 \\ 0 & 0 & 11.3 \end{bmatrix}$	$\begin{bmatrix} -11.50 & 0.91 & 0 \\ 0.91 & -10.3 & 0 \\ 0 & 0 & -4.70 \end{bmatrix}$	$\begin{bmatrix} 28.4 & 0.85 & 0 \\ 0.85 & 2.85 & 0 \\ 0 & 0 & 13.80 \end{bmatrix}$

The constants associated with the transverse shear properties are obtained by procedure described earlier in Section 2.1. The temperature fields, $a_0 = 288$ and $a_1 = 0$; $a_0 = 500$ and $a_1 = 0$; $a_0 = 500$ and $a_1 = 5$ were used to evaluate A_{44}^R and A_{55}^R; A_{44}^T and A_{55}^T; B_{44}^T and B_{55}^T, respectively. The FEM based beam simulations were performed at reference temperature (T_R) to calculate the transverse shear stiffnesses (A_{55} and A_{44}) as shown in Figures 5 and 6. It can be observed that A_{55} and A_{44} are changing with the length of the beam. The value of A_{55} first increases reaches maximum and then gradually decreases with the length of the beam. The maximum value is obtained corresponding to a length of approximately 500 mm. The same length was chosen to evaluate A_{55}^R, A_{55}^T and B_{55}^T. In contrast, the value of A_{44} is decreasing with the length of the beam and is saturated approximately at 1500 mm. For the other simulations to predict A_{44}^R, A_{44}^T and B_{44}^T, the same length of beam was also chosen. The values are shown in Table 5.

Figure 5: Variation of Transverse Shear Stiffness (A_{55}) with the Length of the Cantilever Beam

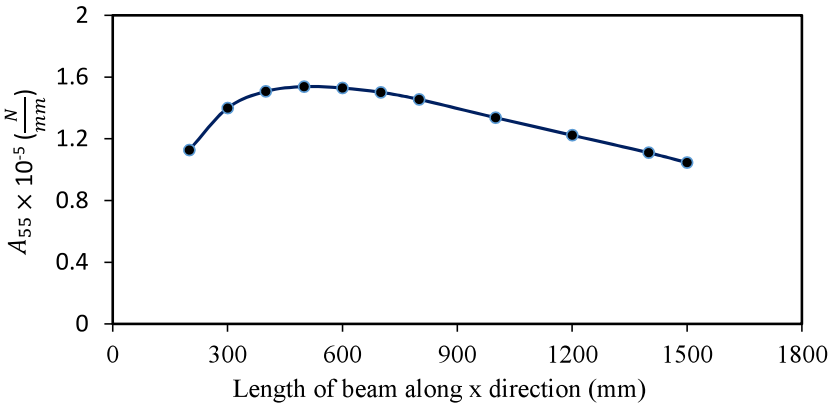

Figure 6: Variation of Transverse Shear Stiffness (A_{44}) with the Length of the Cantilever Beam

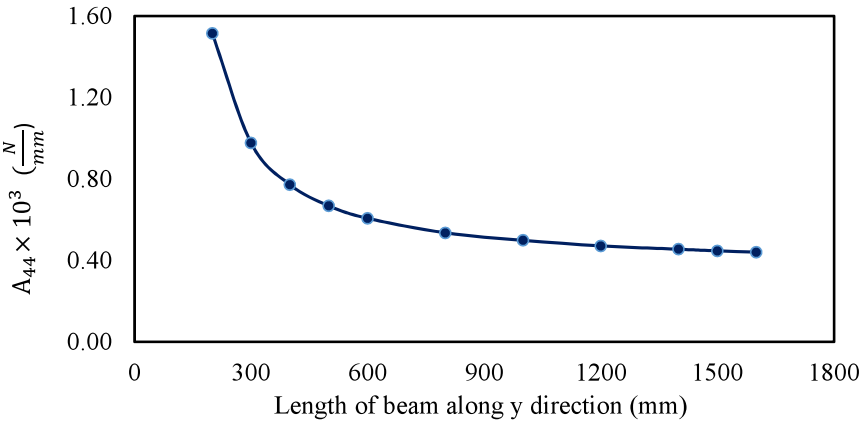

Table 5: Calibrated Transverse Shear Properties at Constant and Linear Temperature Distribution

$A^R_{44}, \frac{N}{mm}$	$A^T_{44}, \frac{N}{mm-K}$	$B^T_{44}, \frac{N}{K}$	$A^R_{55}, 10^5\ \frac{N}{mm}$	$A^T_{55}, \frac{N}{mm-K}$	$B^T_{55}, \frac{N}{K}$
450	-0.27	-0.44	1.54	-93.82	-663.59

Verification of Homogenized Properties with FE Homogenization

For the verification of calibrated constants, as shown in Tables 3 and 4, a thicknesswise temperature field, a_0 = 800 and a_1 = 8 was considered to compute [A], [B] and [D] stiffness properties. The method used to compute the homogenized properties from Equation 11 is termed as "Calibration Method" as shown in Table 6. The unit-cell analyses as discussed earlier were performed to compare with analytically computed stiffness properties and marked out as "Unit-cell Analysis". The accuracy of the proposed method is very close to the unit-cell analysis as shown below in "Error" with the maximum error of 0.36%.

Table 6: Comparison of [A], [B] and [D] with Linear Temperature Variation, T = 800+ 8z.

	$[A], 10^6\ N/mm$	$[B], 10^6\ N$	$[D], 10^6\ N-mm$
Unit-cell Analysis	$\begin{bmatrix} 2.53 & 0.15 & 0 \\ 0.15 & 2.16 & 0 \\ 0 & 0 & 1.0 \end{bmatrix}$	$\begin{bmatrix} -71.14 & -3.80 & 0 \\ -3.80 & -70.24 & 0 \\ 0 & 0 & -33.20 \end{bmatrix}$	$\begin{bmatrix} 2.78 & 0.18 & 0 \\ 0.18 & 2.64 & 0 \\ 0 & 0 & 1.23 \end{bmatrix}$
Calibration Method	$\begin{bmatrix} 2.53 & 0.15 & 0 \\ 0.15 & 2.16 & 0 \\ 0 & 0 & 1.0 \end{bmatrix}$	$\begin{bmatrix} -71.20 & -3.80 & 0 \\ -3.80 & -70.30 & 0 \\ 0 & 0 & -33.30 \end{bmatrix}$	$\begin{bmatrix} 2.79 & 0.18 & 0 \\ 0.18 & 2.64 & 0 \\ 0 & 0 & 1.23 \end{bmatrix}$
Error (%)	$\begin{bmatrix} 0 & 0 & 0 \\ 0 & 0 & 0 \\ 0 & 0 & 0 \end{bmatrix}$	$\begin{bmatrix} 0.08 & 0 & 0 \\ 0 & 0.09 & 0 \\ 0 & 0 & 0.30 \end{bmatrix}$	$\begin{bmatrix} 0.36 & 0 & 0 \\ 0 & 0 & 0 \\ 0 & 0 & 0 \end{bmatrix}$

The transverse shear properties (A_{44} and A_{55}) were calculated with the different thicknesswise temperature profiles using the calibrated constants (Table 5) and compared with the FE beam analyses as shown in Table 7. The computed properties from Equation 13 and cantilever beam analyses are termed as "Calibration Method" and "FE Beam Analysis", respectively as shown in Table 7. The relative errors of computed properties are shown below in "Error" with a maximum error of 5.20%.

Table 7: Comparison of Homogenized Transverse Shear Properties with $T = a_0 + a_1 z$

$T = a_0 + a_1 z$		FE Beam Analysis		Calibration Method		Error (%)	
a_0	a_1	$A_{44}, \frac{N}{mm}$	$A_{55}, 10^5 \frac{N}{mm}$	$A_{44}, \frac{N}{mm}$	$A_{55}, 10^5 \frac{N}{mm}$	A_{44}	A_{55}
600	6	359	1.16	363	1.20	1.11	3.45
700	7	332	1.06	336	1.11	1.20	4.72
800	8	304	0.96	308	1.01	1.32	5.20

Verification of Homogenized Properties with Full-scale Model

Additionally, verification of homogenized properties using the calibrated constants was carried out to compare the response of the homogenized plate model with the full-scale model of ITPS panel having the dimension of a =1000 mm and b = 1000 mm, where a and b are the length along and across the corrugation. The full-scale model of ITPS and homogenized plate were discretized with eight-node shell element (S8R) having 54000 and 400 elements, respectively. The Simply supported boundary conditions (SS2) as shown in 7a and 7b were applied such that edges are free to move in the horizontal plane as follow: $u_2 = u_3 = \theta_1 = 0$ at x = constant and $u_1 = u_3 = \theta_2 = 0$ at y = constant.

Figure: 7FE model and Boundary Conditions for (a) ITPS panel, (b) Homogenized plate model

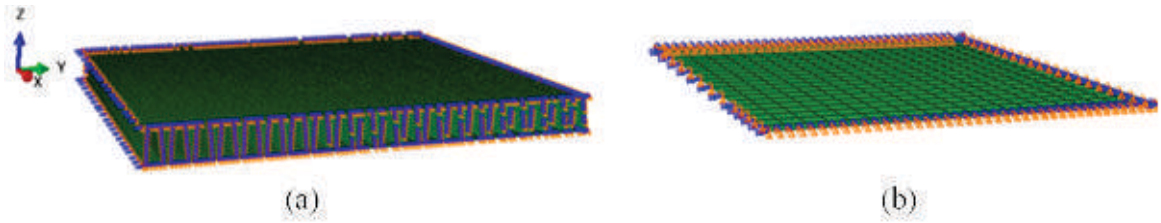

A uniform and spatially varying temperature field were considered to verify the homogenized properties under uniform transverse pressure load applied on the TFS of the ITPS panel and homogenized plate model without consideration of thermal strain. For the spatially varying temperature field, the TFS and BFS are subjected to quadratic distribution as follow:

$T_{TFS} = b_0 + b_1 y + b_2 y^2$ and $T_{BFS} = c_0 + cy + c_2 y^2$ with b_0 =1300 K , b_1 = -0.002 K/mm , b_2 =-0.0005 K/mm^2, c_0 =800 K, c_1 =-0.002 K/mm, c_2 = -0.0005 K/mm^2.

The temperature field for the full-scale model of the ITPS panel was assigned as $T(x, y, z) = a_0(x, y) + a_1(x, y) z$, where a_0 and a_1 were determined from the TFS and BFS temperature variation. For the homogenized plate model, a_0 and a_1 were calculated at the centroid of the corresponding element. The homogenized properties were computed for each element based on the temperature field and assigned using *Shell general Section property card (ABAQUS, 2017).

Mechanical Analyses

To compare the response of the homogenized plate model with the full-scale model of the ITPS panel, the mechanical analyses were performed under uniform and non-uniform temperature filed. The first pair of analyses were carried at a uniform temperature field of T(x, y, z) = 800 K. The second pair of analyses were carried out at a spatially varying temperature field as mentioned before. The contours of the transverse deflection (u_3) at uniform and non-uniform temperature field subjected to a uniform pressure of 101 kPa are shown in Figures 8 and 9. It can be seen from figures that the contours of u_3 of the full-scale model of the ITPS panel and homogenized plate are in good agreement. However, the local deflection can be seen in the full-scale model of the ITPS panel due to the corrugation but these effects are not present in the homogenized plate.

Figure 8: Contour of Transverse Deflection(u_3) of (a) ITPS Panel, and (b)Homogenized Plate at T=800 K

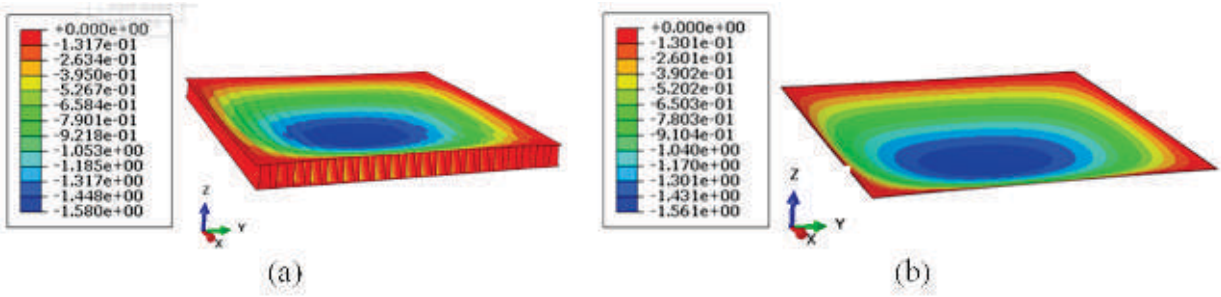

Figure 9: Contour of Transverse Deflection of (a) ITPS Panel, and (b) Homogenized Plate at Spatially Varying Temperature Field

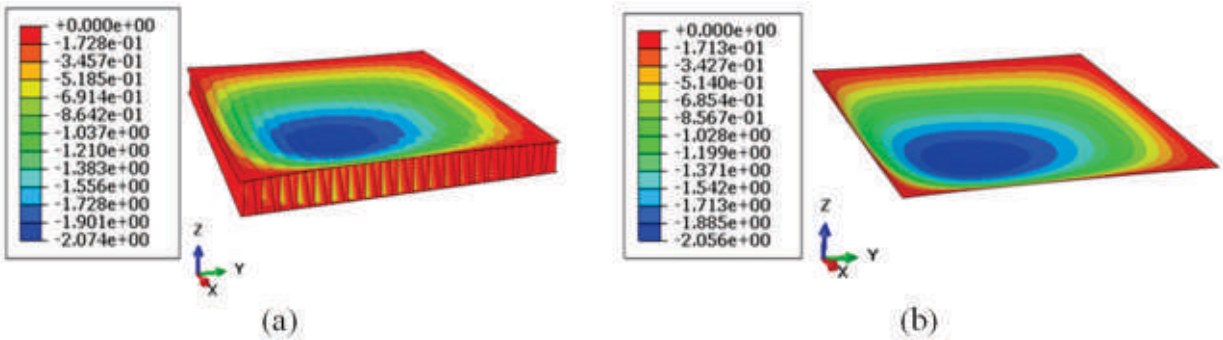

The variation of displacement components of the full-scale model and homogenized plates along x = a/2 and y = b/2 subjected to uniform transverse pressure and temperature of 101 kPa and 800 K, respectively are shown in Figures 10 to 13.

For the comparison with the homogenized plate, the mid-plane of the full-scale model is considered. It can be seen from Figures 10 and 11 that the discrepancy in the error of u_3 and u_2 along the corrugation occurs near the simply supported boundary. The variation in displacement components converges approximately at 200 mm and 800 mm away from the simply supported boundary. From the comparison, it can be seen that boundary oscillations and error in u_2 are larger as compare to u_3. These errors may be attributed to the loss of periodicity creating a localized effect. In contrast, variation in u_3 and u_1 across the corrugation as shown in Figures 12 and 13 matches well near as well as away from the boundary. From these figures, it is clear that boundary oscillations are absent in the full-scale model in contrast to Figures 10 and 12 along the corrugation.

Figure 10: Comparison of u_3 along the Corrugation of Homogenized plate and ITPS Panel

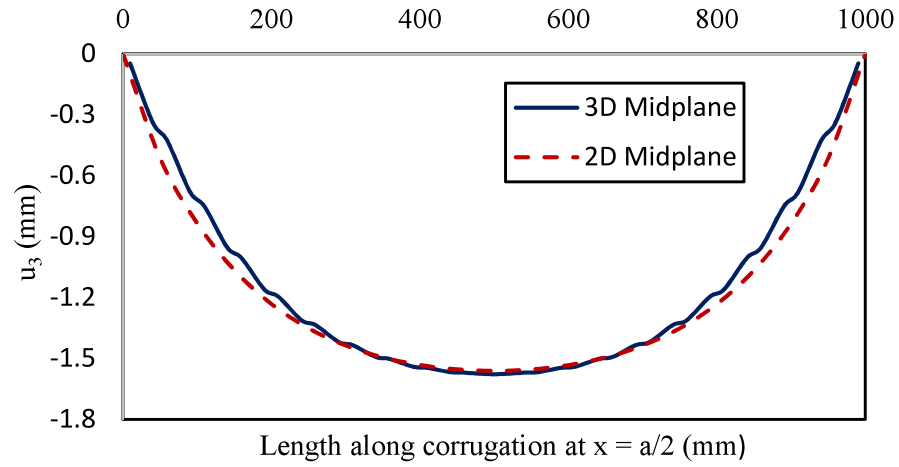

Figure 11: Comparison of u_2 along the Corrugation of Homogenized plate and ITPS Panel

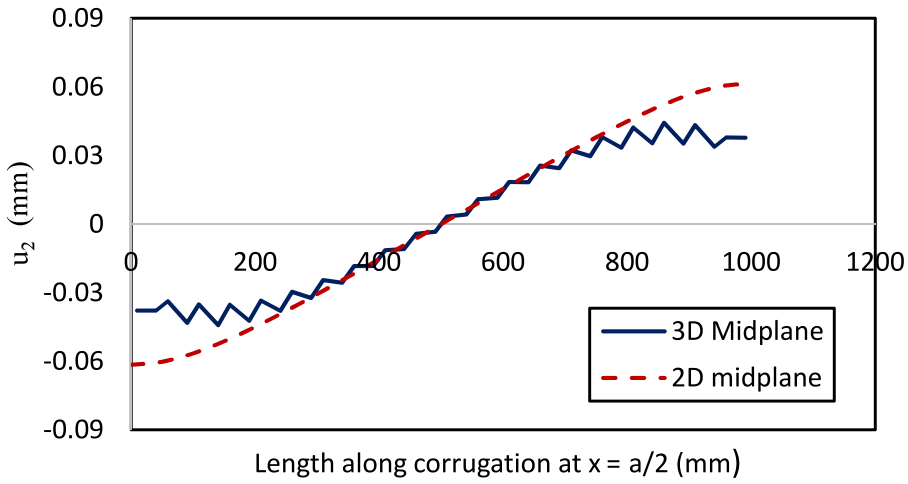

Figure 12: Comparison of u_3 across the Corrugation of Homogenized plate and ITPS Panel

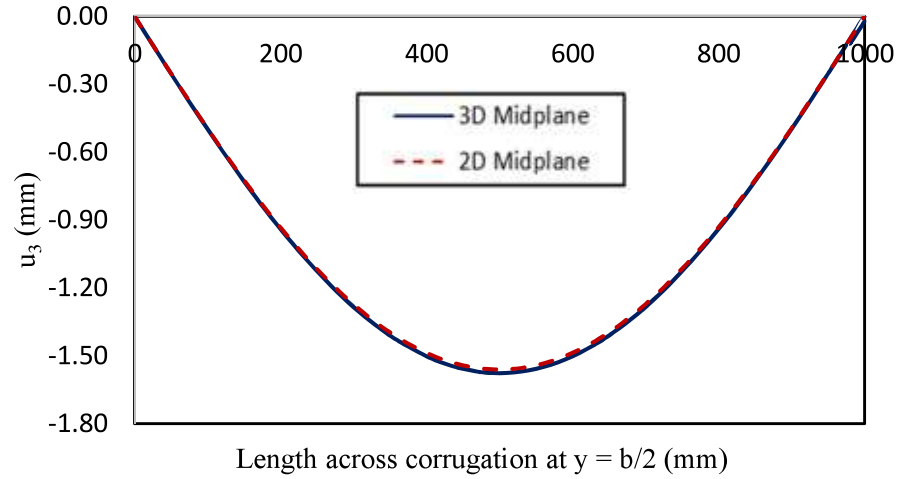

Figure 13: Comparison of u_1 across the Corrugation of Homogenized plate and ITPS Panel

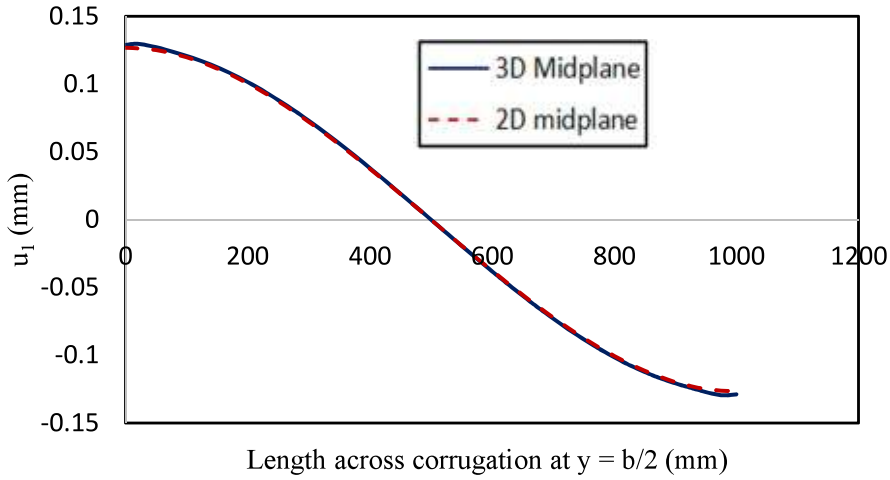

The deviation in error seen along and across the corrugation is due to the sectional geometries in these directions. The plane section remains plane is not an appropriate assumption along the corrugation due to non-uniform geometry. Due to this plate assumption, a large error can be seen along the corrugation. While sectional geometry along y = b/2 is uniform along the length. Thus, error in displacement components is smaller than along the corrugation and acts nearly as a homogenized plate.

Furthermore, the comparison of displacement components between the full-scale model of the ITPS panel and homogenized plate subjected to the non-uniform temperature field and uniform pressure are shown in Figures 14 to 17. It can be observed from Figures 14 and 15 that the variation of displacement components under a non-uniform temperature field is asymmetric in contrast to uniform temperature (Figures 10 and 11). This asymmetry exists due to spatially varying temperature field along the x-direction. However, significant deviations can be seen near the boundary at the location of the applied large temperature field. This inaccuracy can be associated with the error appeared in the transverse shear properties with increasing the temperature. The larger fluctuations in u_2 as shown in Figure 15 can be seen as compared to the previous case of uniform temperature field due to increasing the compliant behavior at higher temperatures, which induced the local bending effect to a greater extent. However, u_2 converges away from the boundary. The magnitude of fluctuations decreases along the corrugation because of the reduction in the applied temperature field.

Figure 14: Comparison of u_3 along the Corrugation of Homogenized plate and ITPS Panel

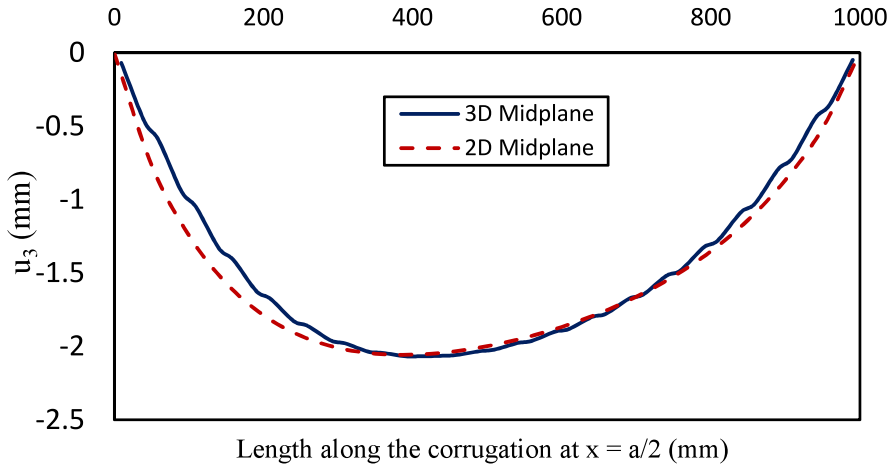

Figure 15: Comparison of u_2 along the Corrugation of Homogenized plate and ITPS Panel

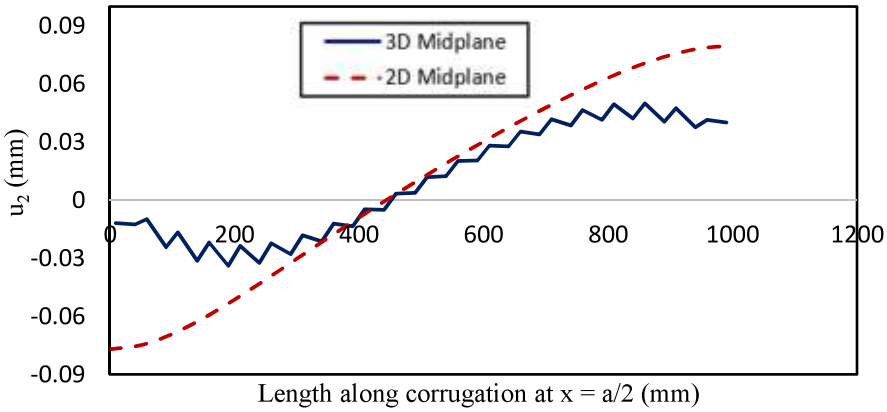

However, a qualitatively similar trend can be seen in the variation of displacement components (u_3 and u_1) along y = b/2 as compared to the previous case of uniform temperature. The variation of u_3 and u_1 are symmetric as shown in Figures 15 and 16 due to the constant temperature field. From the comparison, it can be observed that variation of u_3 and u_1 converges with good accuracy at both near as well as away from the boundary. As discussed earlier, the plate representation across the corrugation is more accurate in contrast to along the corrugation.

Figure 16: Comparison of u_3 across the Corrugation of Homogenized plate and ITPS Panel

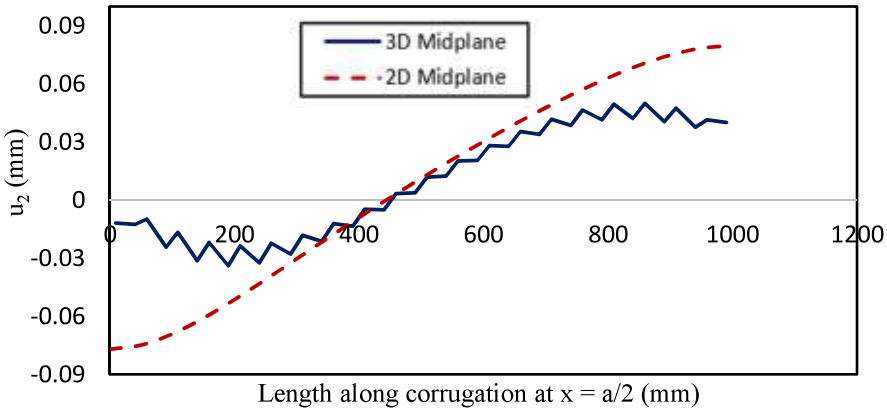

Figure 17: Comparison of u_1 along the Corrugation of Homogenized Plate and ITPS Panel

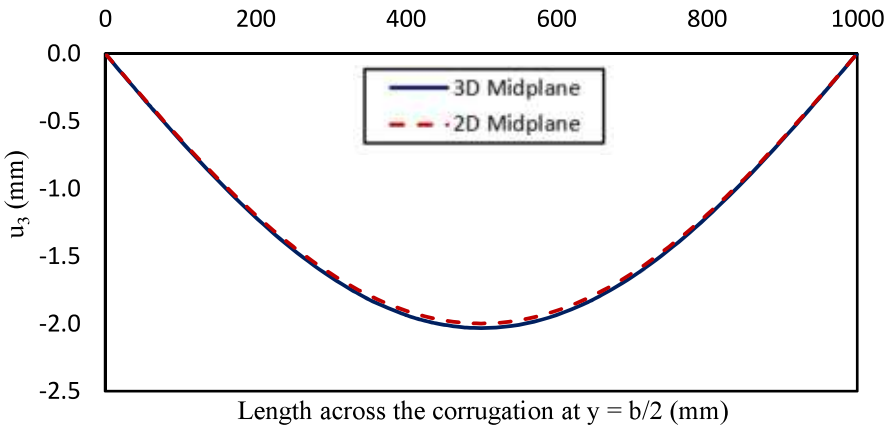

Further, the variations of the strain components of the face-sheets were obtained from the homogenized plate solutions and compared with the full-scale model of ITPS panel. The normal strain components of the TFS and BFS can be evaluated from the plate solution using the kinematic relations as follow:

$\varepsilon_{11} = \varepsilon_{01} + zk_1;\ \varepsilon_{22} = \varepsilon_{02} + zk_2;\ \varepsilon_{12} = \varepsilon_{012} + zk_{12}$

Where $\varepsilon_{01}, \varepsilon_{02}$ and ε_{012} are mid-plane strain components and k_1, k_2 and k_{12} are mid-plane curvatures.

The comparison of strain components (ε_{11} and ε_{22}) of the TFS and BFS along at x = a/2 and y = b/2 under the non-uniform temperature field subjected to uniform pressure as shown in Figures 18 to 21 are compared with the solution obtained from the homogenized plate as described earlier.

The in-plane strain components of TFS and BFS obtained from the plate solutions along x = a/2 are compared with the full-scale model. It can be seen from Figure 18, variation in ε_{11} of the BFS is more accurately predicted by the homogenized plate as compared to the TFS. This may be due to the localized bending effect, which is increasing significantly with temperature. The applied high-temperature field on the TFS enhances the localized effect as compared to the BFS, thus creating large deviations between the plate solutions and the full-scale model. As seen in Figure 19, oscillations in ε_{22} are present for the TFS of the full-scale model due to the web effect and matches with the plate solution in an average sense. However, these oscillations are absent in the BFS due to highly stiff material as compared to the TFS.

It is evident from the comparison along y = b/2 as shown in Figure 20 that the variations in ε_{11} are accurately predicted by the homogenized plate. However, it can be observed from Figure 21 that deviation in ε_{22} of TFS is more as compare to the BFS. These large deviations are due to localized effects as discussed earlier, which are significantly large for the TFS. However, it can be observed from Figures 18 to 21 that strain component (ε_{11}) in the transverse direction to the corrugation is more accurate than ε_{22}. These deviations may be the localized effect, which becomes significant due to the flexible nature of the web.

Figure 18: Comparison of Strain component (ε_{11}) of Homogenized plate and ITPS Panel

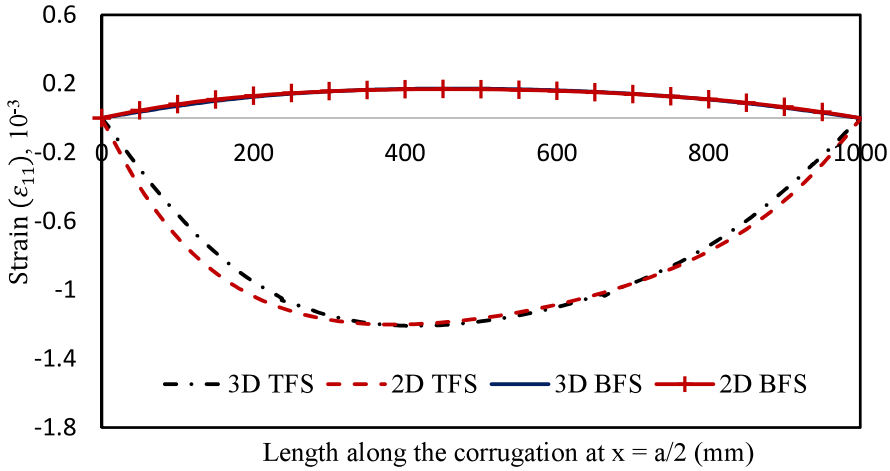

Figure 19: Comparison of Strain component (ε_{22}) of Homogenized plate and ITPS Panel

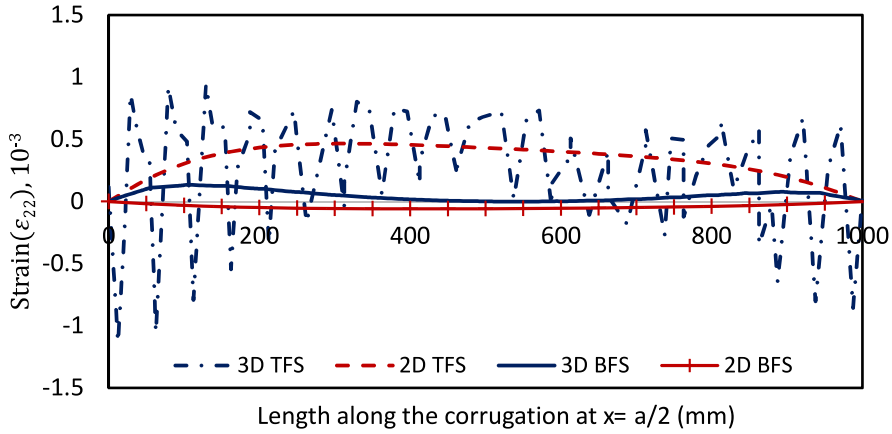

Figure 20: Comparison of Strain component (ε_{11}) of Homogenized plate and ITPS Panel

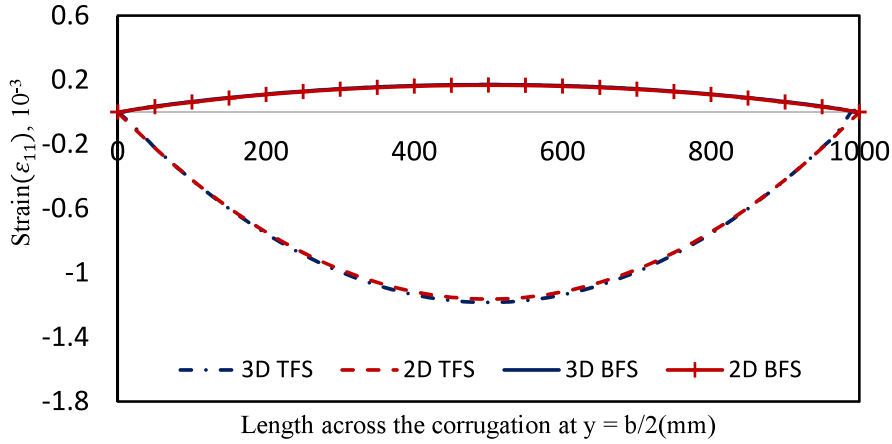

Figure 21: Comparison of Strain component (ε_{22}) of Homogenized plate and ITPS Panel

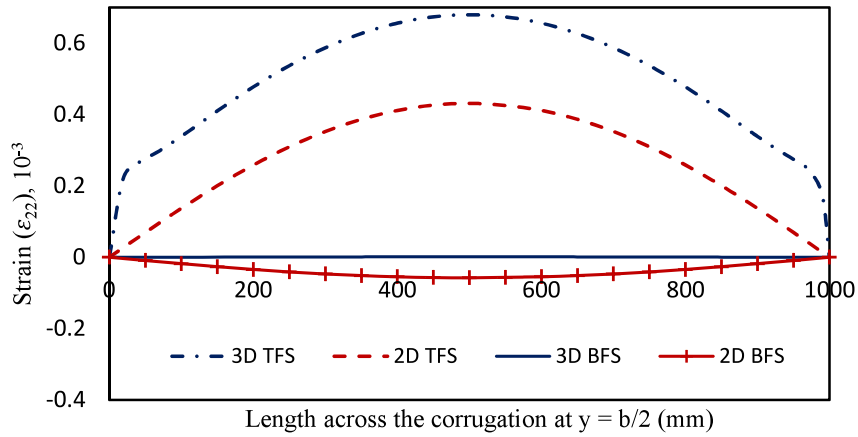

Conclusion

In this paper, the homogenization of ITPS panel as an orthotropic thick plate has been derived with a thicknesswise temperature gradient. The plate representation requires the prediction of the homogenized properties using unit-cell and FEM based beam analyses. The homogenized properties are obtained by calibrating the properties depending upon the thicknesswise temperature variation. The calibration step requires twelve unit cell simulations for extensional ([A]), coupling ([B]) and bending ([D]) matrices, and six FEM based beam analyses for transverse shear (A_{44} and A_{55}) stiffness properties considering constant and linear thicknesswise temperature variation. Once calibrated, any linear thicknesswise variation of temperature can be considered for the homogenous plate model to capture the response of the actual ITPS panel. The homogenized procedure derived in this work can be amplified for a higher order of temperature polynomial, which will require some additional constant be calibrated.

The efficacy of the calibrating procedure has been verified by comparing the homogenized properties with FE homogenization. The in-plane, coupling and bending stiffness properties are approximately the same as micro-mechanical analysis, and the transverse shear stiffness properties have been obtained with a maximum error of 5.20% to exemplify the accuracy of the proposed method.

Furthermore, the response of the homogenized plate model has been verified with the full-scale model of the ITPS panel under both uniform and non-uniform temperature field subjected to uniform transverse pressure. The comparisons of displacement and strain components clearly show that the homogenized plate model yields the results with reasonable accuracy. The full-scale model of ITPS panel and homogenized plate consists of 155452 and 1281 nodes, respectively. Therefore, the total number of degrees of freedom of the ITPS panel is 121 times larger than the homogenous model. Thus, it can be concluded that the homogenization method derived in this work provides computationally efficient solutions and hence can be used in the structural analysis of RLVs.

Future Work

The spatially varying temperature field in ITPS panel necessitates the incorporation of the thermal expansion in the homogenous model. In future, thermomechanical study will be conducted for the corrugated core sandwich structure represented as a homogenized plate model.

References

- ABAQUS, C. (2017). Analysis user's manual.
- Bapanapalli, S. K. (2007). Design of an integral thermal protection system for future space vehicles (Doctoral dissertation, University of Florida).
- Bekey, I., Powell, R., & Austin, R. (1994). NASA studies access to space. *AeAm*, *32*(5), 38-43.
- Carlsson, L. A., Nordstrand, T., & Westerlind, B. O. (2001). On the elastic stiffnesses of corrugated core sandwich. *Journal of Sandwich Structures & Materials*, *3*(4), 253-267.
- Chang, W. S., Ventsel, E., Krauthammer, T., & John, J. (2005). Bending behavior of corrugated-core sandwich plates. *Composite structures*, *70*(1), 81-89.
- Collier, C. (1993, January). Stiffness, thermal expansion, and thermal bending formulation of stiffened, fiber-reinforced composite panels. In *34th Structures, Structural Dynamics and Materials Conference* (p. 1569).
- Craig, S. (1994). Thermoelastic Formulation of Stiffened, Unsymmetric Composite Panels for Finite Element Analysis of High Speed Aircraft.
- Fung, T. C., Tan, K. H., & Lok, T. S. (1993, January). Analysis of C-core sandwich plate decking. In *The Third International Offshore and Polar Engineering Conference*. International Society of Offshore and Polar Engineers.
- Fung, T. C., Tan, K. H., & Lok, T. S. (1994). Elastic constants for Z-core sandwich panels. *Journal of Structural Engineering*, *120*(10), 3046-3055.
- Li, H., Ge, L., Liu, B., Su, H., Feng, T., & Fang, D. (2020). An equivalent model for sandwich panel with double-directional trapezoidal corrugated core. *Journal of Sandwich Structures & Materials*, *22*(7), 2445-2465.
- Libove, C., & Hubka, R. E. (1951). Elastic constants for corrugated-core sandwich plates.
- Martinez, O. (2007). *Micromechanical analysis and design of an integrated thermal protection system for future space vehicles* (Doctoral dissertation, University of Florida).
- Martinez, O. A., Sankar, B. V., Haftka, R. T., Bapanapalli, S. K., & Blosser, M. L. (2007). Micromechanical analysis of composite corrugated-core sandwich panels for integral thermal protection systems. *AIAA journal*, *45*(9), 2323-2336.
- Nordstrand, T., Carlsson, L. A., & Allen, H. G. (1994). Transverse shear stiffness of structural core sandwich. *Composite structures*, *27*(3), 317-329.
- Satish, K. B., Oscar, M. M., & Christian, G. (2006). Analysis and design of corrugated-core sandwich panels for thermal protection systems of space vehicles.
- Sharma, A., Sankar, B., & Haftka, R. (2010, April). Homogenization of plates with microstructure and application to corrugated core sandwich panels. In *51st AIAA/ASME/ASCE/AHS/ASC Structures, Structural Dynamics, and Materials Conference 18th AIAA/ASME/AHS Adaptive Structures Conference 12th* (p. 2706).
- Tan, K. H., Montague, P., & Norris, C. (1989). Steel sandwich panels: finite element, closed solution, and experimental comparisons, on a 6 m x 2. 1 m panel. *Structural Engineer*, *67*, 159-66.
- Yang, J. S., Li, D. L., Ma, L., Zhang, S. Q., Schröder, K. U., & Schmidt, R. (2019). Numerical static and dynamic analyses of improved equivalent models for corrugated sandwich structures. Mechanics of Advanced Materials and Structures, 26(18), 1556-1567.

Nazim Khan *received his Bachelor's degree in Aero-mechanical stream from Aeronautical Society of India, New Delhi in 2011 and Master's degree in Aerospace Engineering from IIT Chennai in 2013. He worked as CAE analyst in Detroit Engineered Product, Chennai (2013-2016). Currently, he is pursuing his Ph.D. in the Department of Aerospace Engineering at IIT Kanpur. His areas of interest are finite element analysis, multi-scale modelling and damage mechanics. He can be reached at nazim@iitk.ac.in*

Pritam Chakraborty *is Assistant Professor in the Department of Aerospace Engineering at IIT Kanpur. He has done his Ph.D. in Mechanical Engineering from The Ohio State University and worked as a Scientist at Idaho National Laboratory, USA, before joining his current role. His interests are in solid mechanics, multi-scale modeling, fatigue, fracture, plasticity and large scale computing. He can be reached at cpritam@iitk.ac.in*